Electron Energy Distributions in a Radiofrequency Plasma Expanded by Permanent Magnets

Tomoyo SASAKI, Kazunori TAKAHASHI, and Tamiya FUJIWARA
Department of Electrical and Electronic Engineering, Iwate University, Morioka 020-8551, Japan

(Received: 30 October 2009 / Accepted: 2 February 2010)

Electron energy probability functions (EEPFs) inside the plasma source expanded by permanent magnets are measured using an rf-compensated probe and a pulsed probe technique, where the plasma is terminated by an electric double layer (DL) near the source exit. The machine has a 6.5-cm-diameter source and a 26-cm-diameter diffusion chamber; a diverging magnetic field is provided by permanent-magnet arrays. In the present experiments, the rf power and the gas pressure are maintained at 250 W and 0.35 – 2.0 mTorr, respectively. In the plasma source upstream of the DL, EEPFs are observed to be Maxwellian up to the break energies corresponding to the potential drop of the DL at the radially central part, and to the sheath voltage of the floating wall at the peripheral part. Above the break energy the EEPFs show the depleted tails; the tail electrons at the central part and near the source wall contribute to neutralizing the DL-induced supersonic ion beam by overcoming the potential drop of the DL, and charging the source wall electrically.

Keywords: radiofrequency plasma, magnetically expanding plasma, permanent magnets, electric double layer, electron energy probability function

1. Introduction

Electric double layers (DLs) consisting of two thin layers with opposite electrical charges create nonlinear plasma-potential structures causing the charged-particle acceleration, deceleration, and reflection [1-3]. The DLs are considered to originate some of the particle accelerations in space, e.g., in aurora zone, in magnetic funnel of the solar corona, and so on [4-6]. In recent laboratory experiments, the DLs have been detected in low-pressure radiofrequency (rf), magnetically expanding plasmas [7]. The investigations on the ion behaviors relating to the DL using retarding field energy analyzers (RFEAs) [8, 9] and a laser induced fluorescence method [10, 11] have demonstrated the presence of supersonic ion beam with energy corresponding to the potential drop of the DL. The behavior of the DL causing the ion acceleration has been well described by a diffusion-controlled-model so far [12, 13]. Regarding the behaviors of the electrons in the magnetically expanding plasmas, on the other hand, recent experiments [14-16] and one-dimensional particle-in-cell (PIC) simulation [17] have shown that the energetic electrons in the upstream of the DL can overcome the potential drop of the DL and neutralize the ion beam. In the series of the experiments, the results on the strength of the DL is about three to seven times of the temperature of the free electrons, which are in fair agreement with another one-dimensional model of the DL, resembling the sheath theory [18].

As to an application of the DL-induced supersonic ion beams, the new type of electric thruster, named the helicon double layer thruster (HDLT), has been suggested [19]. This type of the thruster dose not require any electrodes for the ion acceleration and extraction and a neutralizer; hence it would yield long-life time and make the system simple. In previously reported experiments on the magnetically expanding plasmas containing the DLs, electromagnets are used to generate the steady-state divergent magnetic fields, which consume much electricity and make the devices large and costly. As compact or efficient helicon-plasma sources, the introduction of permanent magnets (PMs) has been attempted recently [20-22]. Some of authors also have suggested a new type of the magnetically expanding plasma source using only the PMs for electrodeless ion acceleration, where the DL formation and the subsequent supersonic ion beam have been detected [23]. Detailed investigations and improvement of the expanding plasma source are progressed now [24-28]. In this source using the PMs and containing the DL, double concentric PMs arrays are employed in order to eliminate the cusp fields and create the constant magnetic field for the plasma production and the expanding magnetic field for the formation of the DL. It is considered that this source is useful for the development of more efficient and compact plasma thruster. From the viewpoint of the application to the thruster, it is important to understand the electron

author's e-mail: kazunori@iwate-u.ac.jp

behaviors in the above-mentioned plasma source expanded by the PMs arrays.

In the present paper, we report the results on the measurements of the electron energy probability functions (EEPFs) inside the plasma source terminated by the DL in the magnetically expanding plasma using PMs.

2. Experimental Setup

The experimental setup is schematically shown in Fig. 1(a), which has already been described in Ref. [23]. The machine has a 20-cm-long and 6.5-cm-diameter glass tube (source tube) terminated by a floating plate at the left end and connected contiguously to a 30-cm-long and 26-cm-diameter grounded diffusion chamber, where $z = 0$ is defined as the interface between the source tube and the diffusion chamber. Here, x, y, and z axes are defined as indicated in Fig. 1(a) and the distance from the z axis on the x-y plane is defined as r. The chamber is evacuated to a base pressure 2×10^{-6} Torr by a diffusion/rotary pumping system, and the argon gas is introduced from the source side through a mass flow controller. The argon gas pressure P_{Ar} is maintained at 0.35 - 2 mTorr in the present experiment. An inductively coupled rf plasma is excited by a double-turn loop antenna surrounding the source tube ($z = -9$ cm) and powered from an rf generator of frequency 13.56 MHz and power 250 W through an impedance matching circuit.

Double concentric arrays consisting of sixteen Neodymium Iron Boron (NdFeB) magnets (10 cm in length, 1.5 cm in width, and 0.5 cm in thickness) are mounted around the source tube in order to generate the axially constant magnetic field near the antenna for the plasma production and the expanding magnetic field near the source exit for the DL formation, where all of the magnets have inward magnetization in the radial direction. The detailed configuration of the magnets has been described in Ref. [23]. The calculated axial component B_z of the local magnetic-field strength are shown in Fig. 1(b). z-y profile of the magnetic-field lines in the source tube is also shown in Fig. 1(c), where the bold lines delineate the field lines terminating on the floating walls of the source exit at $z = 0$ cm. The constant field of about one hundred Gauss is generated over the distance of 7 cm (-13 cm $< z <$ -6 cm) and the field is divergent near the source exit, where the field strength decreases to a few gauss in the middle of the diffusion chamber. Under these conditions, the DL is generated at the diverging-field area ($z = -3$ - 1 cm) and the subsequent ion beam is detected in the downstream side of the DL, i.e., in the diffusion chamber [23].

It is well known that the EEPF is proportional to the second derivative of the I-V curve of a cylindrical Langmuir probe [29]. The measurement of the EEPF in an rf plasma is difficult because the presence of rf electric

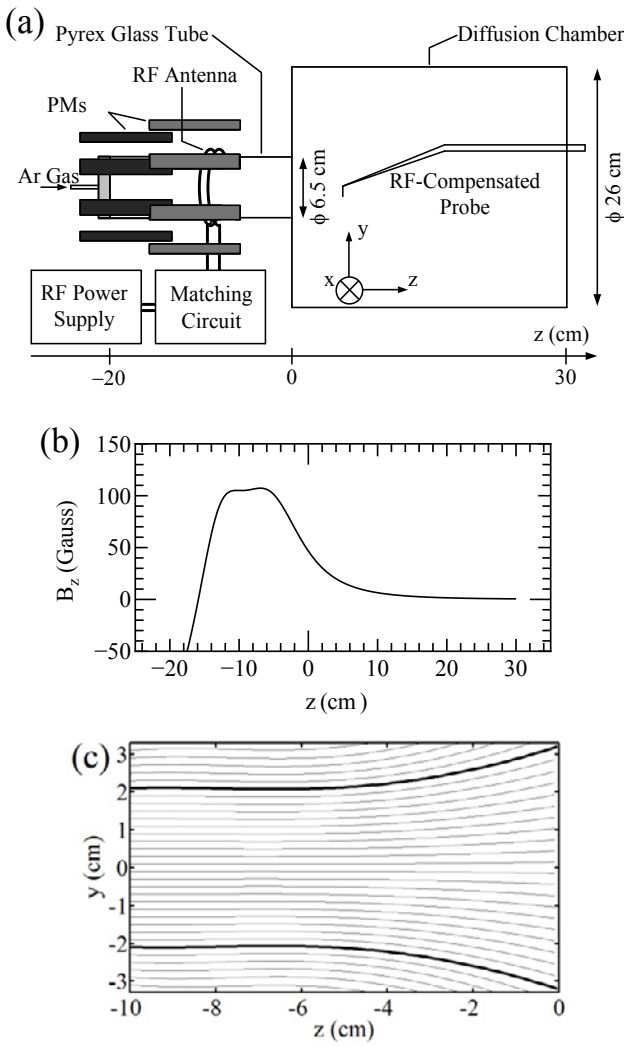

Fig. 1 (a) Schematic diagram of experimental setup. (b) Axial profile of the calculated axial component B_z of the local magnetic-field strength produced by the PMs arrays mounted around the source tube. (c) z-y profile of the magnetic-field lines in the source tube, where the bold lines delineate the field lines terminating on the floating walls of the source exit at $z = 0$ cm.

fields severely distorts the I-V curve of the conventional Langmuir probe [30]. For the present experiment, an rf-compensated cylindrical Langmuir probe (CP) with 3-mm-long and 0.1-mm-diameter tip, which is designed following Ref. [31], is used to measure the EEPFs. The probe is inserted from the downstream side of the diffusion chamber and is movable two-dimensionally. In order to eliminate the influence of the magnetic fields on the I-V curve, the tip radius (0.05 mm) of the CP is smaller than the Larmor radius (~ 0.5 mm) of electrons in the source tube ($B_z \sim 100$ Gauss) [32]. The second derivative of the I-V curve of the CP is directly obtained by a pulsed probe technique using active analog circuit described in Ref. [14, 33]. A 5.5-mm-diameter stainless steel disk is set on the left-side floating plate for the measurement of the wall potential.

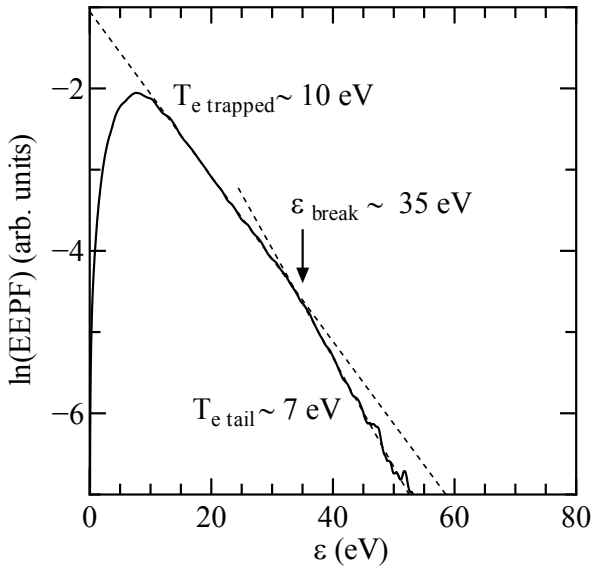

Fig. 2 Natural logarithm plot of electron energy probability function (EEPF) for P_{Ar} = 0.6 mTorr at z = –5 cm and r = 0 cm. The dashed lines show the tangential lines giving each electron temperature $T_{e\,trapped}$ (~10 eV) and $T_{e\,tail}$ (~7 eV). The break energy ε_{break} of the EEPF depletion is indicated by arrow.

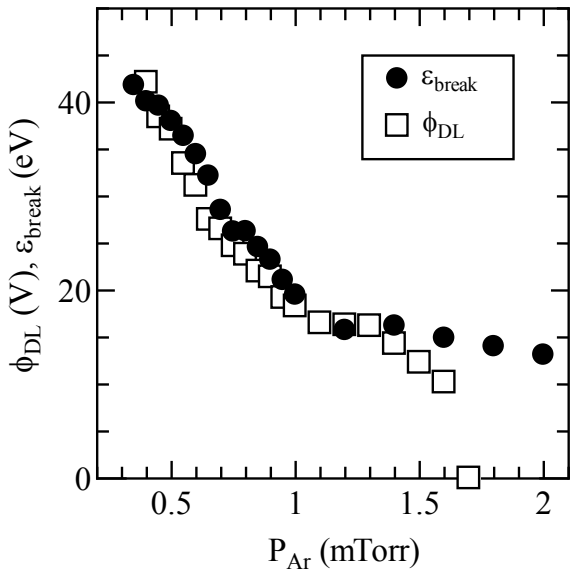

Fig. 3 The break energy ε_{break} (closed circles) of the central EEPF and the potential drop ϕ_{DL} of the DL (open squares) as a function of the argon gas pressure P_{Ar}. The experimental data on ϕ_{DL} are from Ref. [28].

3. Experimental Results and Discussion

The EEPF measured at the central part of the source tube (z = –5 cm and r = 0 cm) is plotted in Fig. 2, where the slope of the EEPF gives us an electron temperature if the slope shows a straight line. The observed EEPF is Maxwellian up to the break energy ε_{break} at about 35 eV and shows a depletion for high energies. Below ε_{break}, the slope of the EEPF yields a electron temperature of about 10 eV, whereas the temperature is about 7 eV above ε_{break}. The break energy ε_{break} in Fig. 2 is in good agreement with the ion beam energy and the potential drop of the DL measured by the RFEA [28].

The break energy ε_{break} and the potential drop ϕ_{DL} of the DL as a function of the argon gas pressure P_{Ar} are plotted in Fig. 3 as closed circles and open squares, respectively, where the experimental results on ϕ_{DL} are from Ref. [28]. Over the range of the argon gas pressure P_{Ar} wherein the DL is generated and the ion beam is detected (P_{Ar} < 1.7 mTorr), the break energy ε_{break} is found to track the potential drop ϕ_{DL} of the DL, which gives us the confidence that the break energy ε_{break} correlates with the potential drop ϕ_{DL} of the DL. For pressures greater than about 1.7 mTorr, the ε_{break} is still observed and remains constant at about 14 eV in spite of the DL dissipation. According to Ref. [34], the high-pressure EEPF-break would originate from inelastic collisions and occur somewhere between the excitation and ionization energies, where the excitation and ionization energies of argon are 11.55 eV and 15.8 eV, respectively. The results are in good agreement with the one-dimensional PIC simulation and the previous experiment [14, 17].

The local plasma potential obtained from the zero crossing point of the second derivative of the I-V curve and the potential of the left-side floating wall are about 68 V and 20 V, respectively. Because the potential drop ϕ_{left} (~ 48 V) of the left-side sheath is larger than the potential drop ϕ_{DL} (~ 35 V) of the DL, the electrons with energies lower than the potential drop of the DL in the upstream area are electrostatically trapped between the DL and the sheath on the left-side floating wall. These electrons are heated by the rf fields for the plasma production and have a relatively high-temperature population of ~ 10 eV. On the other hand, higher-energy depleted-tail electrons with the temperature of ~ 7 eV can overcome the electrostatic potential barrier of the DL and flow into the downstream area with being decelerated by the DL. These energetic electrons would subsequently be reflected by the sheath on the right-side grounded wall and return to the upstream area with regaining the lost energy. The effects of the rf heating on these electrons is much smaller than those on the trapped electrons, as they spend considerably less time in the heating region compared to the time in the downstream region. Hence, the EEPF upstream of the DL have the break energy ε_{break} corresponding to the potential drop of the DL, where the electron temperatures of the trapped electrons and the energetic electrons with depleted tail are defined as $T_{e\,trapped}$ (~ 10 eV) and $T_{e\,tail}$ (~ 7 eV), respectively. Note that the potential drop (ϕ_{DL} ~ 35 V) of the DL is about five times of the temperature of the tail

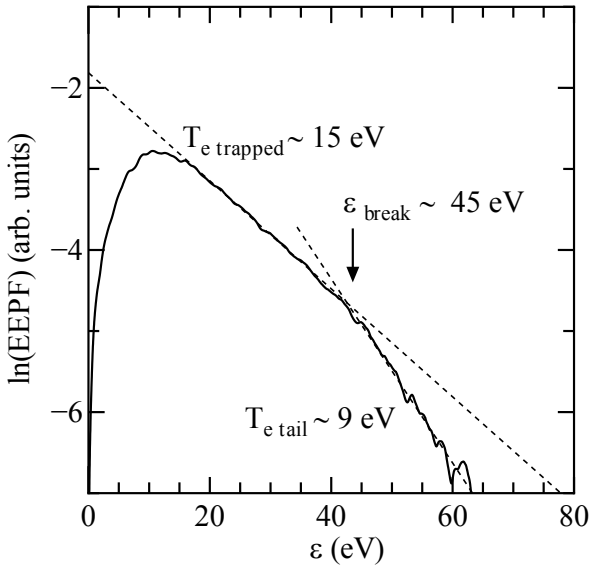

Fig. 4 Natural logarithm plot of electron energy probability function (EEPF) for P_{Ar} = 0.6 mTorr at z = –5 cm and r = 2.2 cm. The dashed lines show the tangential lines giving each electron temperature $T_{e\ trapped}$ (~15 eV) and $T_{e\ tail}$ (~9 eV). The break energy ε_{break} of the EEPF depletion is indicated by arrow.

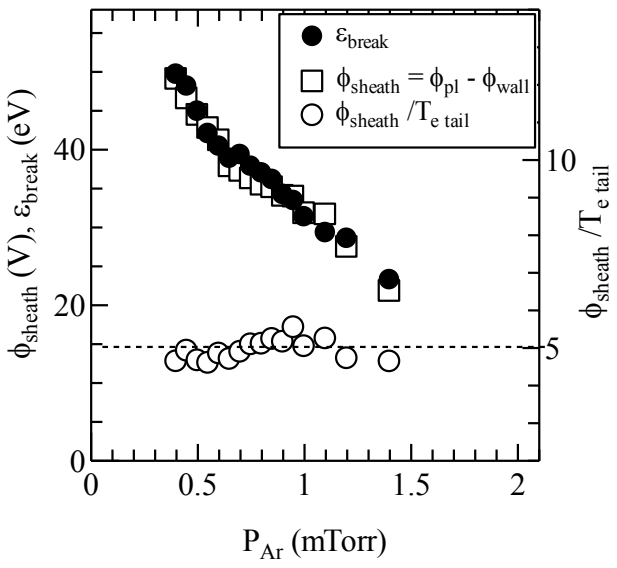

Fig. 5 The break energy ε_{break} (closed circles) of the peripheral EEPF, the sheath voltage ϕ_{sheath} (open squares) on the source wall, and the ratio ϕ_{sheath} / $T_{e\ tail}$ (open circles) as a function of the argon gas pressure P_{Ar}.

electrons ($T_{e\ tail}$ ~ 7 eV) which can pass through the DL. These results are very similar to the previous ones in the different machine using electromagnets [14]. Based on the above-described consideration, it is found that the energetic electrons act as particles neutralizing the ion beam accelerated by the DL in the PMs-expanded plasma as well as the other experiments [14].

The EEPF measured at the peripheral part of the source tube (z = –5 cm and r = 2.2 cm) is also plotted in Fig. 4, where the electron temperatures $T_{e\ trapped}$ (~ 15 eV) and $T_{e\ tail}$ (~ 9 eV), and the break energy ε_{break} (~ 45 eV) are higher than those of the EEPF measured at the central part of the source tube plotted in Fig. 2. Because an Electron cyclotron frequency (~ 280 MHz) in the source tube is considerably higher than a frequency for electron-neutral collision (~ 5.34 MHz), the electrons can be transported along the magnetic-field lines. As shown in Fig. 1(c), the electrons at (z, r) = (–5 cm, 2.2 cm) are on the magnetic-field lines terminating on the floating walls of the source exit at z = 0 cm. Hence, these electrons reach not the DL but the sheath on the source wall. Thus, the break energy ε_{break} in Fig. 4 is expected to relate to the sheath voltage on the source wall [15]. The sheath voltage on the left-side wall can be estimated as 45 V from the difference between the local plasma potential (65 V) in the source and the wall (20 V). It is found that the break energy ε_{break} in Fig. 4 is in good agreement with the estimated sheath voltage.

The break energies ε_{break} of the peripheral EEPFs for various argon gas pressures P_{Ar} are plotted in Fig. 5 as closed circles, together with the measured sheath voltage ϕ_{sheath} on the source wall. The break energy ε_{break} is found to track the sheath voltage ϕ_{sheath} as seen in Fig. 5, which would ensure the correlation between the break energy ε_{break} and the sheath voltage ϕ_{sheath}. At the peripheral area beyond the magnetic-field line terminating on the source exit (bold line in Fig. 1(c)), hence, the low-energy electrons with the temperature $T_{e\ trapped}$ would electrostatically be trapped between the source wall and the left-side wall. Then, the trapped electrons can be heated by strong rf fields near the antenna. As a result, the temperature $T_{e\ trapped}$ would show higher value of about 15 eV. Above the break energy ε_{break}, on the other hand, the energetic electrons would contribute to charging the wall electrically. According to Ref. [35], the floating sheath voltage is five times of the electron temperature in argon plasma. The sheath voltage normalized by $T_{e\ tail}$ plotted as open circles in Fig. 5 are found to be in good agreement with the above description.

The peripheral EEPF shows the temperatures $T_{e\ trapped}$ and $T_{e\ tail}$ higher than those at the central area. Now the detailed radial measurements are performed inside the source tube. Fig. 6(a) shows the radial profiles of the electron temperatures $T_{e\ trapped}$ and $T_{e\ tail}$ for P_{Ar} = 0.6 mTorr. At all radial position, the $T_{e\ trapped}$ is found to be higher than the $T_{e\ tail}$, which means that all of the EEPFs show the depleted tail. The result in Fig. 6(a) presents the increase in the temperatures at the peripheral area (|r| >

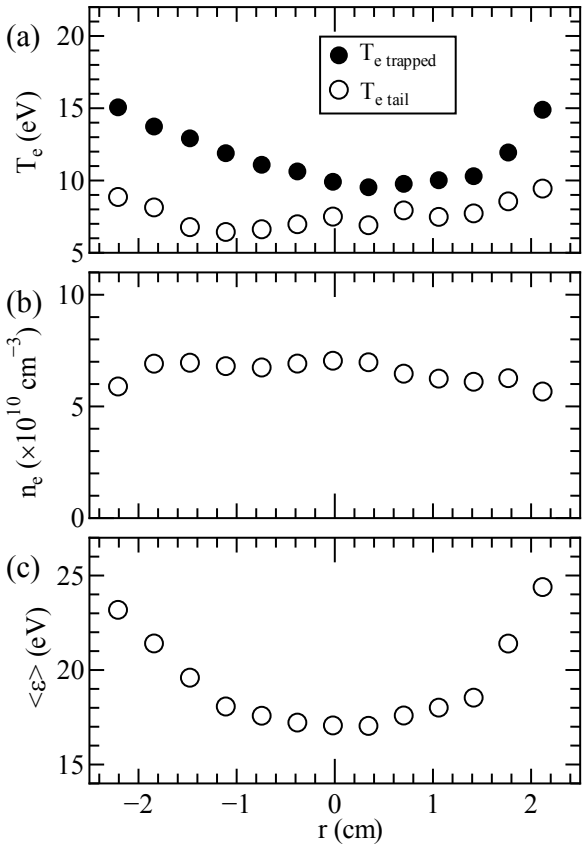

Fig. 6 (a) Electron temperature $T_{e\ trapped}$ (closed circles) and $T_{e\ tail}$ (open circles), (b) plasma density n_e, and (c) the mean energy of electrons $<\varepsilon>$ measured across the source diameter using the rf-compensated probe placed at z = −5 cm, where the argon gas pressure P_{Ar} is 0.6 mTorr.

1.5 cm). In the present experimental system, the rf antenna is winded on the source tube; hence we need to discuss the skin effects of the rf fields. Fig. 6(b) shows the density profile estimated from the integration of the EEPF at each radial position. The result shows the averaged plasma density of about 7×10^{10} cm^{-3}. Under this condition, the skin depth δ can be estimated as $\delta = c / \omega_{pe} \sim 2$ cm, where c and ω_{pe} are the velocity of light and the electron plasma frequency, respectively [36]. Since the inner radius of the source tube is about 3.3 cm, the radial position of the e-folding depth of rf-fields penetration is corresponding to $r \sim 1.3$ cm. Beyond there ($|r| > 1.3$ cm), the temperatures are found to increase gradually in the peripheral area. In order to have a confidence of the rf heating effects on the temperatures, the mean energies of the electrons $<\varepsilon>$ are estimated from the observed EEPFs as plotted in Fig. 6(c). The result clearly indicates the increase in the mean energy of the electrons $<\varepsilon>$ at the peripheral area outer than $|r| \sim 1.3$ cm.

Here, we mention the electron behaviors at the radial central and peripheral part once again. At the central part, the electrons with energy lower than the break energy ε_{break} are electrostatically trapped between the left-side wall and the DL, while the high-energy electrons can overcome the potential drop of the DL and neutralize the ion beam accelerated by the DL. At the peripheral part, on the other hand, the low-energy electrons are trapped between the left-side wall and the glass wall, which are strongly heated by the rf fields near the antenna. The energetic electrons near the source wall are found to contribute to charging the wall electrically, which are transported along the magnetic-field lines terminating on the source exit.

The measurement of the EEPF by the second derivative is generally carried out with the assumption of the isotropic EEPF, while the upstream EEPF would be anisotropic in the present experiment due to the presence of the double-layer electric field. In past studies, the measurements of the electron energy distributions accelerated by the helicon wave through Landau damping process, or by the double layer, were achieved using the second derivative method, where the EEPF would be anisotropic because of the electron acceleration in the axial direction [37, 38]. More recently, the EEPFs in the current-free double layer plasma using electromagnets have been reported and very close to the present results [14, 15]. These results can be reproduced by the one-dimensional PIC simulation [17]. Based on the facts that the present results are consistent with the measured plasma potential [28], with the results in the other machine [14, 15], and with the simulation results [17], the present measurement well describes the electron behaviors.

4. Conclusion

The electron energy probability functions (EEPFs) inside the plasma source expanded by permanent magnets (PMs) are investigated using the rf-compensated probe and the pulsed probe technique, where the plasma is terminated by the electric double layer (DL) near the source exit and the left-side floating wall. In the plasma source upstream of the DL, the EEPFs are observed to be Maxwellian up to the break energies corresponding to the potential drop of the DL at the radially central part, and to the sheath voltage of the floating wall at the peripheral part. Above the break energy, the EEPFs show the depleted tails; At the central part, the electrons with energy lower than the break energy are trapped between the DL and the left-side wall, whereas the higher-energy depleted-tail electrons can overcome the potential drop of the DL and contribute to neutralizing the DL-induced supersonic ion beam. At the peripheral part, the low-energy electrons are trapped between the left-side

wall and the glass wall, whereas the energetic electrons near the source wall contribute to charging the source wall electrically.

Acknowledgements

The authors are indebted to Y. Shida for his technical assistance. This work is partially supported by a Grant-in-Aid for Young Scientists (B, 20740317) from the Ministry of Education, Culture, Sports, Science and Technology, Japan. This work is also partially supported by Yazaki Memorial Foundation for Science and Technology, and the Foundation for the Promotion of Ion Engineering.

[1] B. H. Quon and A. Y. Wong, Phys. Rev. Lett. **37**, 1393 (1976).

[2] G. Hairapetian and R. L. Stenzel, Phys. Rev. Lett. **61**, 1607 (1988).

[3] K. Takahashi, T. Kaneko, and R. Hatakeyama, Appl. Phys. Lett. **91**, 261502 (2007).

[4] R. E. Ergun, Y.-J. Su, L. Andersson, C. W. Carlson, J. P. McFadden, F. S. Mozer, D. L. Newman, M. V. Goldman, and R. J. Strangeway, Phys. Rev. Lett. **87**, 045003 (2001).

[5] D. S. Main, D. L. Newman, and R. E. Ergun, Phys. Rev. Lett. **97**, 185001 (2006).

[6] R. W. Boswell, E. Marsch, and C. Charles, Astrophys. J. **640,** L199 (2006).

[7] C. Charles, Plasma Sources Sci. Technol. **16**, R1 (2007), and references therein.

[8] C. Charles and R. W. Boswell, Phys. Plasmas **11**, 1706 (2004).

[9] N. Plihon, P. Chabert, and C. S. Corr, Phys. Plasmas **14**, 013506 (2007).

[10] S. A. Cohen, N. S. Siefert, S. Stange, R. F. Boivin, E. E. Scime, and F. M. Levinton, Phys. Plasmas **10**, 2593 (2003).

[11] X. Sun, A. M. Keesee, C. Biloiu, E. E. Scime, A. Meige, C. Charles, and R. W. Boswell, Phys. Rev. Lett. **95**, 025004 (2005).

[12] M. A. Lieberman and C. Charles, Phys. Rev. Lett. **97**, 045003 (2006).

[13] M. A. Lieberman, C. Charles, and R. W. Boswell, J. Phys. D: Appl. Phys. **39,** 3294 (2006).

[14] K. Takahashi, C. Charles, R. W. Boswell, T. Kaneko, and R. Hatakeyama, Phys. Plasmas **14**, 114503 (2007).

[15] K. Takahashi, C. Charles, R. W. Boswell, and R. Hatakeyama, Phys. Plasmas **15**, 074505 (2008).

[16] K. Takahashi, C. Charles, R. W. Boswell, and R. Hatakeyama, Appl. Phys. Lett. **94**, 191503 (2009).

[17] A. Meige and R. W. Boswell, Phys. Plasmas **13**, 092104 (2006).

[18] F. F. Chen, Phys. Plasmas **13**, 034502 (2006).

[19] M. D. West, C. Charles, and R. W. Boswell, J. Propul. Power **24**, 134 (2008).

[20] K. P. Shamrai, Y. V. Virko, V. F. Virko, and A. I. Yakimenko, Proceedings of the 42nd AIAA/ASME/ SAE/ASEE Joint Propulsion Conference and Exhibit, California, 2006 (the American Institute of Aeronautics and Astronautics, 2006), p. 4845.

[21] F. F. Chen and H. Torreblanca, Plasma Phys. Control. Fusion **49**, A81 (2007).

[22] F. F. Chen and H. Torreblanca, Phys. Plasmas **16**, 057102 (2009).

[23] K. Takahashi, K. Oguni, H. Yamada, and T. Fujiwara, Phys. Plasmas **15**, 084501 (2008).

[24] K. Takahashi and T. Fujiwara, Appl. Phys. Lett. **94**, 061502 (2009).

[25] K. Takahashi, Y. Shida, T. Fujiwara, and K. Oguni, IEEE Trans. Plasma Sci. **37**, 1532 (2009).

[26] K. Takahashi and T. Fujiwara, to be published in JAXA Research and Development Report (2009).

[27] K. Takahashi, K. Oguni, H. Yamada, and T. Fujiwara, J. Plasma Fusion Res. SERIES **8**, 1269 (2009).

[28] K. Takahashi, Y. Shida, and T. Fujiwara, "Magnetic-field-induced enhancement of ion beam energy in a magnetically expanding plasma using permanent magnets", Plasma Sources Sci. Technol., Submitted.

[29] M. A. Lieberman and A. J. Lichtenberg, *Principles of Plasma Discharges and Materials Processing*, 2nd ed. (Wiley-Interscience, Hoboken, 2005), p. 189-191.

[30] V. A. Godyak, R. B. Piejak, and B. M. Alexandrovich, Plasma Sources Sci. Technol. **1**, 36 (1992).

[31] I. D. Sudit and F. F. Chen, Plasma Sources Sci. Technol. **3**, 162 (1994).

[32] R. R. Arslanbekov, N. A. Khromov, and A. A. Kudryavtsev, Plasma Sources Sci. Technol. **3**, 528 (1994).

[33] K. F. Schoenberg, Rev. Sci. Instrum. **49**, 1377 (1978).

[34] V. A. Godyak, R. B. Piejak, and B. M. Alexandrovich, Plasma Sources Sci. Technol. **4**, 332 (1995).

[35] M. A. Lieberman and A. J. Lichtenberg, *Principles of Plasma Discharges and Materials Processing*, 2nd ed. (Wiley-Interscience, Hoboken, 2005), p. 172.

[36] M. A. Lieberman and A. J. Lichtenberg, *Principles of Plasma Discharges and Materials Processing*, 2nd ed. (Wiley-Interscience, Hoboken, 2005), p. 464.

[37] R. T. S. Chen and N. Hershkowitz, Phys. Rev. Lett. **80**, 4677 (1998).

[38] R. Schrittwieser, I. Axnäs, T. Carpenter, and S. Torvén, IEEE Trans. Plasma Sci. **20**, 607 (1992).